HEAFAT 2014

10th International Conference On Heat Transfer, Fluid Mechanics and Thermodynamics

14-16 July 2014

Orlando, Florida (USA)

Numerical Study of The Effect of Liquid Sloshing Inside TLD on Suppression of Gust Wind- Induced Vibration in High Rise Buildings

Oda T. F.[1,†], Hamed M.S.[1,*], and Saud Ghani[2]

ABSTRACT

Needless to say that the use of TLD in damping of the light scale vibration in due to wind excitation as well as the large scale excitation on offshore platforms exhibits an effective dynamic absorber. One of the prime importance of using TLD as an effective absorber coupled with structure is to impart the effect of fatigue stresses accompanied with the repeated excitation loads. The serviceability of the high rise buildings and the steel towers is another important application of using TLD to suppress the building acceleration and realize the comfort and healthy conditions. The full scale measurements of the structure dynamic response exhibits an effective method for the validation of the structure design procedure and emphasize the accuracy of the numerical models suggested predicting the structure dynamic response. The current model behaves as a NSE model accurately predict the sloshing fluid motion inside TLD and handles the moving free surface by using the (VOF) method. The current model use the continuum surface force model CSF to model the discontinuity accompanied with wave breaking inside TLD. The numerical model used in this paper predicts the interaction between the structure dynamic response and highlights the damping effect of TLD groups allocated at different floors of tall buildings. The current model suggests a new criterion to detect the wave breaking and focus attention on the effect of wave breaking on the impact force in due to the sloshing fluid motion inside TLD for a wide range of excitation frequencies. The numerical model used in this paper handles the interaction between the structure dynamic response and the damping effect of TLD groups allocated at different floors of the tall building. The model was validated by a direct comparison with the full scale measurements of one of the high rise buildings. The direct comparison shows a good agreement proves that the current numerical model is a powerful tool used assess the damping effect of TLD on structure dynamic response.

1 Thermal Processing Laboratory, Department of Mechanical Engineering, McMaster University, Hamilton, Ontario, Canada

[†]Correspondence to : Oda, T.F., E-Mail: tarekrok@gmail.com & tareko@mcmaster.ca

[*]Professor , Director, Thermal Processing Laboratory, Department of Mechanical Engineering, McMaster University, Hamilton, Ontario, Canada , E-Mail: hamedm@mcmaster.ca

2 Professor , Head ,Department of Mechanical and Industrial Engineering, Qatar University, Doha, Qatar, E-Mail: s.ghani@qu.edu.qa

1. INTRODUCTION

The large amplitude excitation induced by gust winds and earthquakes affect greatly the steel high buildings and towers from the serviceability and occupants comfort points of view [1, 2, 3].

The high rise building acceleration performs a sensitive parameter enroll the high rise building serviceability. The recommended value of the building acceleration must not exceed the acceleration threshold, [4].

The accurate experimental evaluation of the tall building model dynamic response conducted in wind tunnels must be calibrated using (CAARC), [5,6].

The use of tune liquid dampers imparts the use of other passive damping devices from the reliability, operating and maintenance costs [7,8]. The use of group of TLD`s was crucial to damp the vibration due to wind excitation especially in the tall buildings [9]. The use of group of TLD's increase the damping ratio as much as five times if compared to the fundamental damping ratio of the structure without liquid storage tanks, as noticed in the Nagasaki airport tower, and Yokohama marine tower [9]. The current numerical model [10] predicts the sloshing motion and tracking the free surface inside TLD using the VOF method as well as using the CSF model to model the driving forces of the liquid free surface inside TLD. On the other hand, the current numerical model predicts high rise building dynamic response for the Structure-TLD interaction model. The current fluid-structure interaction model compared with full scale measurements of the dynamic response conducted in the National Bank of China.

A comparative study conducted of structure dynamic response behaviour in case of using of mass damper coupled with the structure compared with the use of TLD-structure coupling damping system.

Another comparative study explored for the effect of using multi-TLD groups coupled with structure and allocated at the different tall building storeys.

2. LITERATURE REVIEW

Numerous of numerical modeling methods invoked to assess the sloshing behavior of the liquid inside the TLD. In the early studies [11, 12] equivalent mechanical models were suggested for both the structure as well as the liquid storage tanks. On the other hand a different way of handling the liquid sloshing numerically were invoked based on the potential flow theory [13, 14] as well as the shallow water wave theory[15, 16].In fact the potential flow theory has no account for the effect of fluid properties on the sloshing liquid motion. Hence it can not be used to investigate the fluid flow behavior around obstacles as the created vortices could not be modeled via the potential theory. It was crucial to tune the natural frequency of the sloshing motion to be near the natural frequency of the excited structure. Hence the in need to use of NSE numerical model accurately handle the convective – acceleration terms in the momentum equations. The current numerical model classified as a NSE model to predict the sloshing fluid motion inside TLD. The building acceleration constitutes the appropriate parameter to check the building serviceability. The design criteria of tall building states that the acceleration at any floor, at any vibration mode, will not exceed the acceleration threshold that claims good serviceability, [4]. In fact the first step to simulate the wind flow around the building numerically was in due to Hanson et al [17], and Summers et al [18]. The fluid-structure interaction model was analyzed numerically [19, 20] to explore the coupling between the mechanical and aerodynamic forces at the fluid-structure interface.

3. THE CURRENT NUMERICAL MODEL

3.1.The Numerical Model of sloshing liquid inside TLD

The current model built in-house and classified as NSE model. The model solves the momentum equations of the viscous fluid flow inside TLD [10]. The construction of the liquid free surface as well as the re-construction in due to free surface evolution with time is achieved by using VOF method [21, 22].The current model use the continuum surface force model CSF [23] to handle the surface tension forces and the fluid flow stresses gradients nearby the fluid surface interface. On the other hand, the experimental study [24] revealed that the pressure exerted on the walls varies in a similar nature as that of the applied excitation. Accordingly, the current numerical model assign the pressure at the excited TLD tank walls, [10]:

$$p = \alpha p * e^{\left(\frac{-y}{h}\right)} * \sin(\omega t) \quad (1)$$

3.2 The Modelling of Structure Dynamics

The fluid structure interaction model used in this paper will handle the selected floor as a SDOF structure coupled with TLD as a passive damper. The equation of motion of the structure-floor model will be solved using Duhamel's integral method [25]. The tall building, used in the current study, will be simulated as MDOF shear-building model. Moreover, the current numerical study will consider the elastic range of the structure strength in the handling of structure dynamics according to wind flow.

3.3. The Characteristics of the Tall Building Selected for The Current Study

The building total height is 367 m, and includes 70-storey constructed from steel and reinforces concrete. The location of the building is very close to the seashore and on the lee slope of extremely hilly terrain in a typhoon active area [26]. Robertson et al [27] illustrates the detailed structure system of the building.

4. THE GOVERNING EQUATIONS

4.1 The Governing Equations of sloshing fluid inside TLD

The governing equation of the incompressible , Newtonian ,laminar flow in the Cartesian coordinate system has been modeled for the velocity field $\vec{V}$ as a function of space and time as $\vec{V} = u(x,y,t)\hat{i} + v(x,y,t)\hat{j}$, where at any fixed point in the flow field , $\vec{x}$ in the domain $\vec{x} = x\hat{i} + y\hat{j}$ are described using Cartesian Coordinate system as:

4.1.1. Continuity Equation

$$\frac{\partial u}{\partial x} + \frac{\partial v}{\partial y} = 0 \qquad (2)$$

4.1.2 The Momentum Equation in X- Direction

$$\frac{\partial u}{\partial t} + u\frac{\partial u}{\partial x} + v\frac{\partial u}{\partial y} = -\frac{1}{\rho}\frac{\partial p}{\partial x} + g_x + \frac{1}{\rho}\frac{\partial \tau_{xx}}{\partial x} + \frac{1}{\rho}\frac{\partial \tau_{xy}}{\partial x} \quad (3)$$

4.1.3 The Momentum Equation in Y- Direction

$$\frac{\partial v}{\partial t} + u\frac{\partial v}{\partial x} + v\frac{\partial v}{\partial y} = -\frac{1}{\rho}\frac{\partial p}{\partial y} + g_y + \frac{1}{\rho}\frac{\partial \tau_{yy}}{\partial y} + \frac{1}{\rho}\frac{\partial \tau_{xy}}{\partial y} \quad (4)$$

4.1.4 The Free Surface Time Evolution Equation

The reconstruction of the free surface using VOF will be based on the donor–acceptor cell method, [22]. The time evolution equation of the liquid free surface was presented as:

$$\frac{\partial F}{\partial t} + u\frac{\partial F}{\partial x} + v\frac{\partial F}{\partial y} = 0 \qquad (5)$$

After the velocity and pressure fields are calculated using an assumed volume of fluid, F, the F-field is updated. The new F-field is calculated by solving equation (5). The conservative form of the F – field, as:

$$\frac{\partial F}{\partial t} + \frac{\partial (F\,u)}{\partial x} + \frac{\partial (F\,v)}{\partial y} = 0 \qquad (6)$$

The donor-acceptor method used, [36] to resolve the sharp interface noticed in the free surface.

4.2. The Boundary Conditions

4.2.1. The Fluid Flow Velocity Components Boundary Conditions at TLD Solid Walls

The no-slip velocity boundary condition, i.e. zero tangential velocity applied at the wall. The normal component of the velocity at the wall is also set to be zero due to non-penetrating wall boundary condition, Figure 1.

4.2.2. The pressure boundary condition at the bottom wall

The pressure at the fluid cells in the vicinity of the ghost cells of the bottom wall will have a pressure which equals to the hydrostatic pressure of the fluid and according to the nominal fluid height.

4.2.3. Pressure boundary condition at left and right walls

The left and right walls ghost cells will copy the weavy pressure equation on the neighbouring fluid cells. Hence the formulae used in the handling of pressure at the left and right TLD walls will be according to the experimental findings [24];

$$p = \alpha p * e^{\left(\frac{-y}{h}\right)} * \sin(\omega t) \qquad (1)$$

4.2.4 Fluid Flow Stresses boundary conditions at tank walls

According to the no-slip condition at tank solid boundaries, as the general viscous stress tensor:

$$\tau_{ik} = \mu\left(\frac{\partial u_i}{\partial x_k} + \frac{\partial u_k}{\partial x_i}\right) \qquad (7)$$

Then the normal stress as well as the shear stresses will be vanished at the solid boundaries of the TLD.

4.2.5 The Free Surface Boundary Condition

The CSF model used suggest a transition region with finite depth at the interface region between the water surface (fluid 1) and air adjacent (fluid 2), [23]. The two fluids are characterized by a function, $c(\vec{x})$ which was:

$$\begin{aligned} c(\vec{x}) &= c_1 \quad , for\ \ fluid(1) \\ &= c_2 \ , for\ \ fluid(2) \\ &= \langle c \rangle = (c_1 + c_2)/2 \ \ , at\ the\ \text{int}erface \end{aligned} \qquad (8)$$

The fluid density at any point in the transition region evaluated as $\rho(\vec{x}) = \langle \rho \rangle$. The CSF model replaces the discontinuous characteristic function $c(\vec{x})$ by a smoothed variation function, $\tilde{c}(\vec{x})$ of the fluid properties from c_1 to c_2 . This variation will be demonstrated over a distance $o(h^*)$, where (h^*) is the transition layer thickness and comparable to the resolution afforded by the calculation mesh size. The exact surface stress boundary condition at the free surface in tensor form [23], as:

$$(\sigma\kappa - p_s)\hat{n}_i = (\delta_{ik} - \hat{n}_i\hat{n}_k)\frac{\partial \sigma}{\partial x_k} - \tau_{ik}\hat{n}_k \quad (9)$$

Where σ is the fluid surface tension, $\hat{n}_i$ is the unit force normal to the surface (into fluid 2), and $\kappa(\vec{x})$ is the local free surface curvature, taken positive if the center of curvature points towards (fluid 2), Figure 2. The projection of the surface stress in tensor form, equation (9) along the unit normal $\hat{n}$ and the unit tangent $\hat{t}$ results in ,[23]:

$$p_s - \sigma\kappa = 2\mu n_k \frac{\partial u_k}{\partial n} \qquad (10)$$

The tangential boundary condition given by:

$$\mu\left(t_i \frac{\partial u_i}{\partial n} + n_k \frac{\partial u_k}{\partial s} \right) = \frac{\partial \sigma}{\partial s} \qquad (11)$$

Where, $\frac{\partial}{\partial s} = \hat{t}.\nabla$ is the surface derivative and $\frac{\partial}{\partial n} = \hat{n}.\nabla$ is the normal derivative.

Numerous of numerical techniques neglect the viscous stress on the R.H.S of equation (10) as the surface tension, equation (10) as well as its gradient, equation (11) constitute the dominant part to induce the pressure jump across the fluid interface. The current model use the CSF model to reformulate the surface tension using the volume force $\vec{F}_{sv}$ and by using the delta function, as:

$$\lim_{h\to 0} \int_{\Delta V} \vec{F}_{sv}(\vec{x})\, d^3x = \int_{\Delta S} \vec{F}_{sa}(\vec{x}_S)\, dS \qquad (12)$$

Where $\vec{x}_S$ is a point on the interfacial area ΔS. The integration of volume force $\vec{F}_{sv}$ around the volume of the interfacial transition region was, according to the Green Theorem, equal to the integration of the surface force $\vec{F}_{sa}$ around the interfacial area ΔS. Then:

$$\vec{F}_{sa}(\vec{x}_S) = F_S^{(n)}\,\hat{n} + F_S^{(t)}\,\hat{t} \qquad (13)$$

Where $F_S^{(n)}$ and $F_S^{(t)}$ are the surface force components along the unit normal ($\hat{n}$) and the unit tangent ($\hat{t}$) respectively, Figure 2. In the current numerical work the viscous stresses at the free surface were neglected and the surface tension coefficient σ was assumed to be constant, Hence:

$$\vec{F}_{sa}(\vec{x}_S) = \vec{F}_s^{(n)}(\vec{x}_S) = \sigma\,\kappa(\vec{x}_S)\,\hat{n}(\vec{x}_S) \qquad (14)$$

The surface tension force per unit interfacial area $\vec{F}_s^{(n)}(\vec{x}_S)$ will be added to the body force in the momentum equation:

$$\frac{\partial \vec{V}}{\partial t} + \nabla.\left(\vec{V}\vec{V}\right)^n = -\frac{1}{\rho}\nabla p + \frac{1}{\rho}\nabla.\tau + \vec{g} + \frac{1}{\rho}\vec{F}_b \qquad (15)$$

5. THE NUMERICAL IMPLEMENTATION

5.1 The Use of the Two Steps Projection Method to Divide the Momentum Equation

The time discretization form of the momentum equation for incompressible fluid flow will be:

$$\frac{\vec{V}^{n+1} - \vec{V}^n}{\delta t} = -\nabla.\left(\vec{V}\vec{V}\right)^n - \frac{1}{\rho^n}\nabla p^{n+1} + \frac{1}{\rho^n}\nabla.\tau^n + \vec{g}^n + \frac{1}{\rho^n}\vec{F}_b^n \qquad (16)$$

It follows that two step projection method follow to divide the momentum equation (15) into:

$$\frac{\tilde{\vec{V}} - \vec{V}^n}{\delta t} = -\nabla.\left(\vec{V}\vec{V}\right)^n + \frac{1}{\rho^n}\nabla.\tau^n + \vec{g}^n + \frac{1}{\rho^n}\vec{F}_b^n \qquad (17)$$

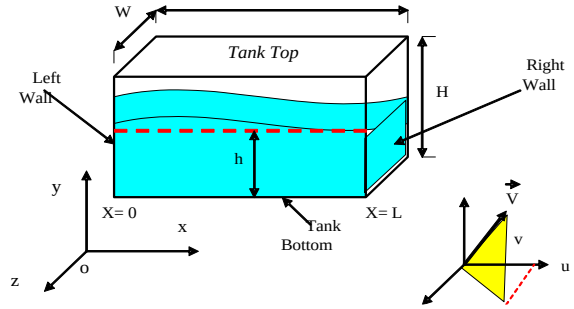

Figure 1. The TLD Basic Dimensions

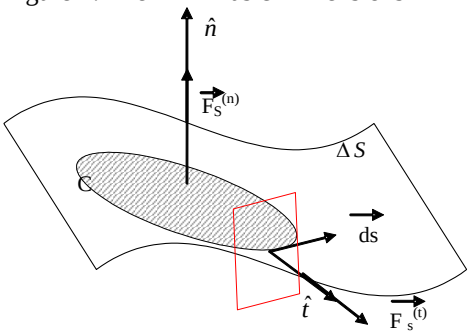

Figure 2. The Normal and Tangential Surface Force Components at the Free Surface

AND $$\frac{\vec{V}^{n+1} - \tilde{\vec{V}}}{\delta t} = -\frac{1}{\rho^n}\nabla p^{n+1} \qquad (18)$$

The virtual velocity field $\tilde{\vec{V}}$ at the previous time step, will be corrected by the pressure gradient term at the new time step to extract the new velocity field vector at the new time step, { $\vec{V}^{n+1}$ }, equation (18). Moreover, the continuity equation:

$$\nabla.\vec{V}^{n+1} = 0 \qquad (19)$$

Combine equation (18) with equation (19) we extract Poisson's equation, for evaluation of pressure gradient, as:

$$\nabla.\left(\frac{1}{\rho^n}\nabla p^{n+1}\right) = \frac{\nabla.\tilde{\vec{V}}}{\delta t} \qquad (20)$$

5.2 The Numerical Algorithm

The non-conservative form of the momentum advection $\frac{\partial \vec{V}}{\partial t}$,through the control volume boundaries was given by:

$$\frac{\partial \vec{V}}{\partial t} = -\left(\vec{V}.\nabla\right)\vec{V} \qquad (21)$$

While the conservative form of the momentum advection;

$$\frac{\partial \vec{V}}{\partial t} = -\nabla.\left(\vec{V}\vec{V}\right) \qquad (22)$$

The computational cell for the x-direction and y-direction momentum equation illustrated in figure (3) and figure (4) respectively, while the computational cell dimensions were illustrated in figure (5).

The current numerical model use the Van Leer limiter to improve the accuracy of upstream approximation by retaining second order terms in Taylor's expansion.

5.3. The Computation Time Step and Stability Criterion

The momentum transport equation (16) and the free surface time evolution equation (5) according to the VOF method were explicit equations in time. Hence the calculation time step must be criticized by the Courant time limit;

$$\delta t \le \left\{ \delta t_C = \min\left(\delta t_{cx} , \delta t_{cy} \right) \right\}$$

And $$\delta t_{cx} = C \left\{ \frac{\delta x}{|u|} \right\}_{\min.} , \delta t_{cy} = C \left\{ \frac{\delta y}{|v|} \right\}_{\min.} \quad (23)$$

The value of {C = 0.3} to ensure stability [7,29]. The current numerical time step chosen to be $\delta t = 6.62 * 10^{-4}\ Sec.$

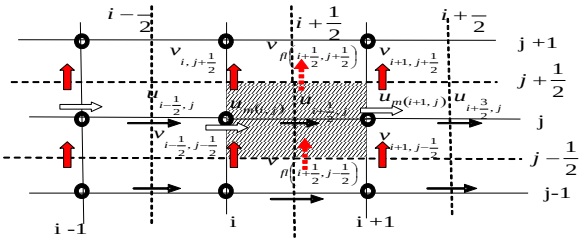

Figure 3. The Computational Cell of X-Direction Momentum Equation

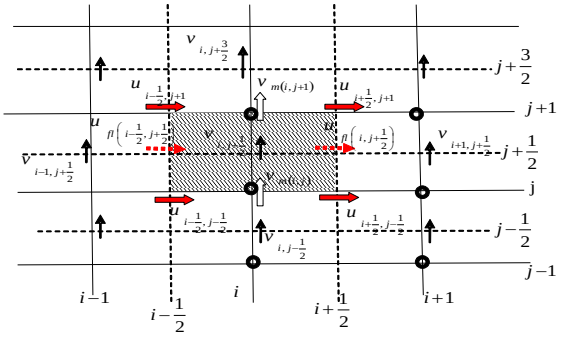

Figure 4. The Computational Cell of Y-Direction Momentum Equation

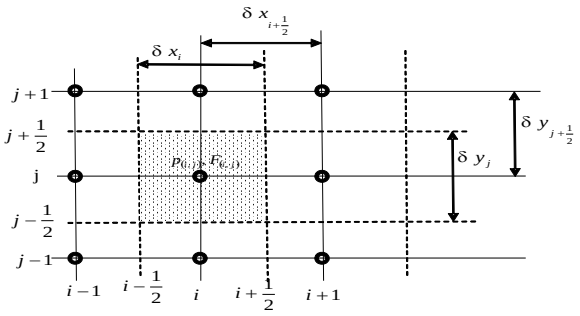

Figure 5. The computation Grid Basic Dimension

5.4. The Numerical Model of Fluid- Structure Interaction

The equation of horizontal motion of the fluid-structure system, which modeled as SDOF system and formulated,[30]:

$$M_S \ddot{X}_S + C_S \dot{X}_S + K_S X_S = F_{TLD} + F_{excitation} \quad (24)$$

M_S : The generalized mass of the equivalent SDOF model, C_S : The generalized damping coefficient, K_S is the generalized stiffness coefficient, X_S , $\dot{X}_S$ and $\ddot{X}_S$ are the structure displacement, velocity, and acceleration in x-direction, respectively.

$F_{excitation}$: The external excitation force affects the structure. F_{TLD} : The sloshing motion impact force on the TLD walls, in x-direction and modeled as:

$$F_{TLD} = \frac{1}{\Delta t} \left(mom(t) - mom(t + \Delta t) \right) \quad (25)$$

The integral method used in the current study is the Duhamel's integral method [25]. The total displacement of the damped SDOF model given by :

$$X_S(t) = e^{-\xi \omega_n t} \left(X_0 \cos \omega_D t + \frac{u_0 + X_0 \xi \omega_n}{\omega_D} \sin \omega_D t \right) \quad (26)$$

Moreover the total force acts on the structure at any time instant (τ) during the time period $(0 \to t)$;

$$F_{tot}(\tau) = F_{excitation}(\tau) + F_{TLD}(\tau) \quad (27)$$

The particular solution of the structure equation of motion

$$X_S(t) = \frac{1}{M_S \omega_D} \int_0^t F_{tot}(\tau) e^{-\xi \omega_n (t-\tau)} \sin \omega_D (t-\tau) \, d\tau \quad (28)$$

The structure displacement at time (t_i):

$$X_S(t_i) = \frac{e^{-\xi \omega_n t_i}}{M_S \omega_D} \left[A_D(t_i) \sin \omega_D t_i - B_D(t_i) \cos \omega_D t_i \right] \quad (29)$$

Where: $A_D(t_i)$, and $B_D(t_i)$ are evaluated using the recurrence relations, [7,8,35]. The detailed computations of the Duhamel integrals could be reviewed in [7, 8,35].

6 THE STRUCTURE DYNAMIC CHARACTERISTICS

6.1. The Structure Natural Frequencies

The structure selected a 70-storey building has a height of 367 m, and the structure system was illustrated in details in [27]. The structure was modeled as a shear-model with five lumped masses and 15 degrees of freedom [26, 31], Figure 6. The measured natural frequencies of the first and second vibration modes were 0.307 Hz and 0.334Hz,[32, 33]. In the current model we select the frequency of structure as 0.32 Hz.

6.2. *Field Measurements of Structure Dynamic Response Parameters*

The full scale measurements conducted on the structure [32, 33] by using two accelerometers fitted at the 68th floor, as well as two Gill type propeller anemometers mounted atop of the structure. The collected measured data are; the acceleration, the wind speed, and the wind direction time histories. The cross spectral density of the along –wind response forces were expressed, [4, 27, 34, and 35] as:

$$S_{u_i u_j}(z_i, z_j, n) = C_D{}^2 \rho^2 \bar{V}_{10}^2 h_i h_j \left(\frac{z_i}{10}\right)^{\alpha} \left(\frac{z_j}{10}\right)^{\alpha} * S_V(n) \int_{B/2}^{B/2} \int_{B/2}^{B/2} coh(y_i, y_j, z_i, z_j, n) dy_i dy_j \quad (30)$$

z_i and z_j : The elevation of the i[th] and j[th] floors from the ground level, respectively.

h_i and h_j : The height of the i[th] and j[th] floors respectively.

C_D : The wind flow drag coefficient, [64].

ρ : The air density, $\rho = 1.225 kg/m^3$, [27].

$S_V(n)$: The power spectrum of the wind speed, estimated using Von-Karman spectrum and the Davenport spectral function [34].

$coh(y_i, y_j, z_i, z_j, n)$: The coherence function, defined as a narrow band correlation corresponding to in-phase components at a frequency (n).

$$coh(y_i, y_j, z_i, z_j, n) = \exp\left(-\frac{2n\left\{C_y^2 (y_i - y_j)^2 + C_z^2 (z_i - z_j)^2\right\}^{\frac{1}{2}}}{\bar{V}(z_i) + \bar{V}(z_j)}\right) \quad (31)$$

C_y and C_z : The decay coefficients in y and z direction respectively, $C_y = 16$, and $C_z = 10$,[4].

The detailed computation are illustrated in [35].

6.3. The Current Numerical Modelling of Along Wind Response Forces

The along –wind force power spectrum, equation (30) will be expressed on the time history domain using the trigonometric function [36] as:

$$F_{R,AlongWind}(t) = \sum_{k=1}^{k_n} \left(\left(\frac{2}{T} S_{u_i u_j}(z_i, z_j, n_k)\right)^{\frac{1}{2}} \cos(2\pi n_k t + \psi_k) \right) \quad (32)$$

k : The number of division of the frequency.

n_k : The frequency of the upcoming wind.

$F_{R,AlongWind}(t)$: The wind response force induced along the wind flow direction.

T : The duration time span.

ψ_k : The phase difference.

Moreover by using equation (32) with the aid of equations (30, 31), then the time domain of the generalized excitation force, $F_{excitation}(t)$ will be estimated using EUROCODE I, [37], as:

$$F_{excitation}(t) = C_S \cdot C_D \cdot C_F \cdot q(z_e) \cdot A_{ref} \quad (33)$$

The force coefficient, C_F , the structural coefficient, C_S , the drag coefficient, C_D , will be evaluated using [37].

Thereafter the current numerical model evaluates the structure dynamic response parameters, using Duhamel integrals.

7. THE FLOW CHART OF THE CURRENT NUMERICAL MODEL

The details of the numerical algorithm illustrated in Figure 7.

8. NUMERICAL MODEL VALIDATION

The TLD tank was excited with sinusoidal excitation with amplitude (A= 0.1 m), and of frequency (f = 1.0 Hz), [38]. The time history of the dimensionless free surface elevation detected numerically compared with experimental work [38], Figure 8. Figure 8 exhibits good compatibility between the numerical model and the experimental findings clears the verification of the use of the current numerical model to detect the free surface evolution of the sloshing liquid inside TLD in case of the hydraulic jump and wave breaking.

9. RESULTS AND DISCUSSIONS

9.1. The numerical Prediction of the Wind- Induced Dynamic Responses of a Tall Building

The simulated along-wind forces fit to the current numerical code to evaluate the dynamic response of the structure induced by wind flow based on the simple shear model, in which the tall building considered as MDOF shear-building model. The current numerical model accurately estimates the generalized mass of the equivalent SDOF, [39] to investigate the dynamic building characteristics at the location of the selected floor. The current numerical model will consider the elastic range of the structure strength in the handling of structure dynamics according to wind flow. The structure- damping ratio selected to be constant, $\xi = 0.56\%$ is considered in the current paper.

9.2. The numerical Prediction of the time history of structure Acceleration induced by the wind flow Random excitation atop the High Rise Building

In fact the most structure dynamic parameter assists the structure vibration limit and safety are tidily related to the structure acceleration.

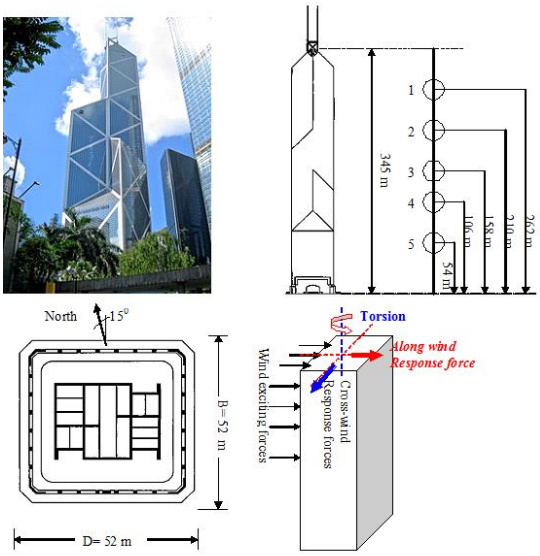

Figure 6. Over view of the National Bank of China
(a) Photo of the tower resides in Hong Kong, [4, 27].
(b) The distribution of building lumped masses, [27].

Hence, the structure acceleration in x- direction time history was detected by the numerical technique, at the location of 68th floor, Figure 9. The direct examination of Figure 9 shows good compatibility with the measurements [27], which implies that the current model accurately detect the structure dynamic response parameters.

9.3. The Effect of TLD on the damping of Structure Dynamic Response

The three natural frequencies of the tall building are 0.311, 0.329, and 0.468 Hz, which were all below 1.0 Hz. Hence the tall building must be considered as a flexible structure. Consequently, in order to prohibit the structure dynamic response, we must use a group of TLDs positioned on the structure floors. The selected floor to be investigated are located at lumped mass (3), 158m from the ground.

9.3.1. The Effect of TLD on Damping Structure Acceleration

In order to investigate the damping effect of TLD on structure acceleration, the acceleration ratio time history, introduced as the ratio between structure acceleration in case of structure-TLD coupling to that of the un-damped structure, figure (10). A group of (10) TLD's used allocated at 158m above the ground level. The examination of figure(10) shows that the use of TLD will make a reduction on the structure dynamic response acceleration over the time period selected.

9.3.2. The Numerical Prediction of PSD of the Structure Acceleration

Figure 11 represents the Numerical Prediction of PSD of the Structure Acceleration as (10 TLDs activated), for a structure frequency of 0.32 Hz. The PSD of the acceleration of the structure-TLD coupling system, Figure 11 shows a peak signal at the structure natural frequencies, a fact that assists the TLD damping effect on the structure acceleration at the different vibrational modes. However, the overwhelming effect of using passive dampers as a group of TLD`s over the classical TMD must be checked.

9.4. A Comparative Study of TLD-Structure Damping effect Compared to TMD Damping Devices.

The paramount damping effect of the TLD over the TMD used for suppression the wind-induced vibration in tall buildings will be investigated. We introduce a parameter called the force response ratio which is a ratio between the response force of the damping device in due to the wind excitation and the response force of the un-damped structure;

$$FRR = \frac{F_{\text{Response, Damping Device}}}{F_{\text{Total Bared Structure Response}}} \quad (34)$$

The analysis of the structure dynamic response in case of structure coupling with different damping devices will be investigated through the power spectrum diagram of the force response ratio. Figure (12) represents the power spectrum diagram of the force response ratio for a tuned mass having the value of the total mass of the (10) TLD`s group, and moves with the structure acceleration and attached to the structure at the location of lumped mass (3), 158m above the ground level. The examination of figure (12) reveals that the effect of TMD attached to the structure will be noticeable for the first third natural frequency (0.456 Hz) of the selected high rise building. On the other hand, the numerical prediction of PSD of the FRR of activated (group of 10 TLD's) attached to the high rise building at a level of 158m high of ground level was illustrated in figure (13). Figure (13) shows a peak of PSD signal at the first natural frequency of the structure as well as he second and third natural frequencies. This finding claims that the use of TLD dampers will be effective for a broad ban of structure natural frequencies. Moreover the direct comparison between figure (12) and figure (13) shows that the value of FRR in due to TLD dampers will outweigh the values of FRR for the use of TMD, a fact that highlights the overwhelming benefit of using TLD dampers to suppress the wind-induces vibration in high rise buildings.

10. CONCLOUSIONS

The use of TLD in damping of the light scale vibration in due to wind excitation outweighs the other passive damping

devices. The current numerical model classified as a NSE model accurately handle the free surface evolution by using VOF method to reconstruct the free surface coupled by using the CSF model to handle the volume fluid force caused by surface tension. The current numerical model suggests a new formula for a dynamic boundary of pressure at the tank side walls. The structure serviceability and integrity behaves as indispensable parameter to be considered in the design of tall buildings and towers. The flexible un-damped tall buildings, the steel towers and steel structures are in need to be coupled with damping devices to suppress the structure dynamic response parameters. The current numerical model solve for the structure dynamic response parameters; the structure displacement, velocity, and the structure acceleration.

The current numerical prediction of the sloshing motion inside TLD was in good compatibility of the experimental findings, [38].

The current numerical study reveals that the use of TLD groups with the tall building and allocated at different building storeys will reduce the tall structure acceleration.

A comparative study conducted between the use of TLD dampers and the TMD reveals that the use of TLD as a robust damper for a wide range of tall structures natural frequencies enroll and outweigh the use of any other passive dampers.

11. REFERENCES

1. Fujii K. , Tamura Y. , Sato T. , Wakahara T. Wind-induced vibration of tower and practical applications of tuned liquid damper. *Journal of Wind Engineering and Industrial Aerodynamics*, 1990; **33**: 263-72.

2. Glanville M.J., Kwok K.C.S. Dynamic characteristics and wind induced response of a steel frame tower. *Journal of Wind Engineering and Industrial Aerodynamics*, 1995; **54/55**: 133-149.

3. Cao H., Reinhorn A.M., Soong T.T. Design of an active mass damper for a tall TV tower in Nanjing, China. *Engineering Structures*, 1998; **20:** 134-143.

4. Li Q.S., Wu J.R., Liang S.G., Xiao Y.Q., Wong C.K. Full-scale measurements and numerical evaluation of wind-induced vibration of a 63-storey reinforced concrete tall building. *Engineering Structures*, 2004; **26:** 1779-1794.

5. Tanaka H., Lawen N. Test on the CAARC standard tall building model with a length scale of 1:1000. *Journal of Wind Engineering and Industrial Aerodynamics*, 1986; **25(1)**: 15-29.

6. Goliger A.M., Milford R.V. Sensitivity of the CAARC standard building model to geometric scale and turbulence. *Journal of Wind Engineering and Industrial Aerodynamics*, 1988; **31(1)**: 105-123.

7. M. Marivani, M.S. Hamed, Numerical investigation of Sloshing Motion inside Tuned Liquid Dampers with and without submerged screens", *PhD Thesis, McMaster University*, 2009.

8. M. Marivani and M.S. Hamed, "Numerical Modeling of Sloshing Motion in a Tuned Liquid Damper Outfitted with a submerged Slat Screen", *Int. Journal of Numerical Methods in Fluids*, available on-line January 12, 2010, 22 pages.

9. Tamura Y. ,Fuji K. , Obtsuki P. , Pacheco B.M. Effectiveness of tuned liquid dampers under wind excitations. *Engineering Structures*, 1995; **17**(9):609-621.

10. T.F. Oda, M.S. Hamed, S. Ghani, "On Wave Breaking in Tuned Liquid Dampers", In "9th International Conference of Heat Transfer, Fluid Mechanics, and Thermodynamics, HEFAT2012", Malta, 2012.

11. Abramson, H.N. The dynamic behavior of liquids in moving containers. *NASA SP-106*, National Aeronautics and Space Administration. Washington, DC, 1966.

12. Vandiver J. Kim and Shuhei Mitome. Effect of liquid storage tanks on the dynamic response of offshore platforms. *Applied Ocean Research*, 1979; **1**(2).

13. Nakayama T. , Washizu K. The boundary element method applied to the analysis of two dimensional nonlinear sloshing problems. *International Journal of Numerical Methods In Engineering*, 1981; **17**: 1631-46.

14. Nakayama T. Boundary element analysis of nonlinear water wave problems. *International Journal of Numerical Methods In Engineering*, 1983; **19:** pp. 953.

15. Sun L.M. Semi-analytical model for tuned liquid damper (TLD) with emphasis on damping with liquid sloshing. *Ph.D. Thesis*, University of Tokyo,1991.

16. Tait M.J., El Damatty A.A., Isyumov N. Effectiveness of a 2D TLD and its numerical modeling. *Journal of Structural Engineering*, 2005; **34**:79-96.

17. Hanson T, Smith F, Summers D, Wilson CB. Computer simulation of wind flow around buildings. *Computer-Aided Design*, 1982; **14(1):**27–31.

18. Hanson T, Summers D, Wilson CB. A three-dimensional simulation of wind flow around buildings. *International Journal of Numerical Methods in Fluids*, 1986; **6**:113–27.

19. Rugonyi S., Bathe K.J. On the finite element analysis of fluid flows fully coupled with structural interactions. *Computer Modeling in Engineering & Sciences*, 2001; **2:** 195-212.

20. Swaddiwudhipong S, Khan MS. Dynamic response of wind-excited building using CFD. *Journal of Sound and Vibration*, 2002; **253(4):**735–54.

21. B. D. Nichols, C. W. Hirt, "Proceedings First Intern. Conf. Num. Ship Hydrodynamics", Gaithersburg, Md, October 1975.

22. C. W. Hirt, B. D. Nichols , "Volume of Fluid Method (VOF) Method for the Dynamics of Free Boundaries", J. Comp. Phys., **39**: 201-225, 1981.

23. J. U. Brackbill, D. B. Kothe, C. Zemach, "A Continuum Method for Modeling Surface Tension", Journal of Computational Physics, **100**: 335-354, 1992.

24. P.K. Panigrahy, U.K. Saha, D. Maity, "Experimental studies on sloshing behavior due to horizontal movement of liquids in baffled tanks", Ocean Engineering, **36**: 213–222, 2009.

25. P.E. Raad, D.B. Johnson, S. Chen, "Simulation of impacts of fluid free surfaces with solid boundaries", International Journal of Numerical Methods in Fluids, **19:**153–76, 1994.

26. Q.S. Li, K.E. Yang, C.K. Wong, A.P. Jeary, "The effect of amplitude-dependent damping on wind-induced vibrations of a super tall building", Journal of Wind Engineering and Industrial Aerodynamics, **91**: 1175-1198, 2003.

27. L.E. Robertson, P.A. Zottola , "Structural system of the New Bank of China building, In "Proceedings of the Fourth International Conference on Tall Building", Hong Kong university, Hong Kong, 85-90, 1988.

28. Van Leer Bram, "Towards The Ultimate Conservative Difference Scheme. V. A second Order Sequel to Godunov's Method", Journal of Comp. Physics, **32:** 101-136, 1979.

29. Dongming Liu, Pengzhi Lin, A numerical study of three-dimensional liquid sloshing in tanks. *Journal of Computational Physics*, 2008; **227**:3921-39.

30. M. Tait, "The performance of 1-D and 2-D tuned liquid dampers", Ph.D. Thesis, University of Western Ontario, London, Canada, 2004.

31. A.C. Steckley, G.R. Lythe, N. Isyumov, A.G. Davenport, "Aeroelastic wind tunnel model study of the New Bank of China Building, Hong Kong", Research Report N6A 5B9, Boundary Layer Wind Tunnel Laboratory, The University of Western Ontario, 1985.

32. Q.S. Li, J.Q. Fang, A.P. Jeary, C.K. Wong, D.K. Liu, "Evaluation of wind effects on a super tall building based on full scale measurements", Earthquake Engineering and Structural Dynamics, **29 (12)**:1845–1862, 2000.

33. Q.S. Li, J.Q. Fang, A.P. Jeary, C.K. Wong, Y.W. Chow , "Field measurements of structural responses of a 70-storey tall building under Typhoon conditions", The Structural Design of Tall Buildings, **9:** 325-342, 2000.

34. A.G. Davenport, "Gust loading factors", Journal of Structural Division, ASCE, **93(3):** 11-34, 1967.

35. T.F. Oda, M.S. Hamed, S. Ghani. "On the Damping of Wind–Induced Vibration in Tall Buildings"**,** The 14th Int. Conference on Civil, Structural and Environmental Engineering Computing, Italy Sep 2013.

36. A. Kawaguchi, A. Teramura, Y. Omote, "Time history response of a tall building with a tuned mass damper under wind force", Journal of Wind Engineering and Industrial Aerodynamics, **(41-44):**1949-1960, 1992.

37. Eurocode 1: Actions on Structures. Part 1-4: General Actions–Wind Actions. EN 1991-1-4:2005. April, 2005.

38. A. Colagrossi, C. Lugni, M. Greco, O. Faltinsen, "Experimental and numerical investigation of 2D sloshing with slamming", In" Proc. 19th International Workshop on Water Waves and Floating Body", Cortona, Italy, 2004.

39. B. Ganjavi, H. Hao , "Elastic and inelastic response of single-and multi-degree-of-freedom systems considering soil structure interaction effects", Australian Earthquake Engineering Society 2011 Conference, Barossa Valley, South Australia, 2011.

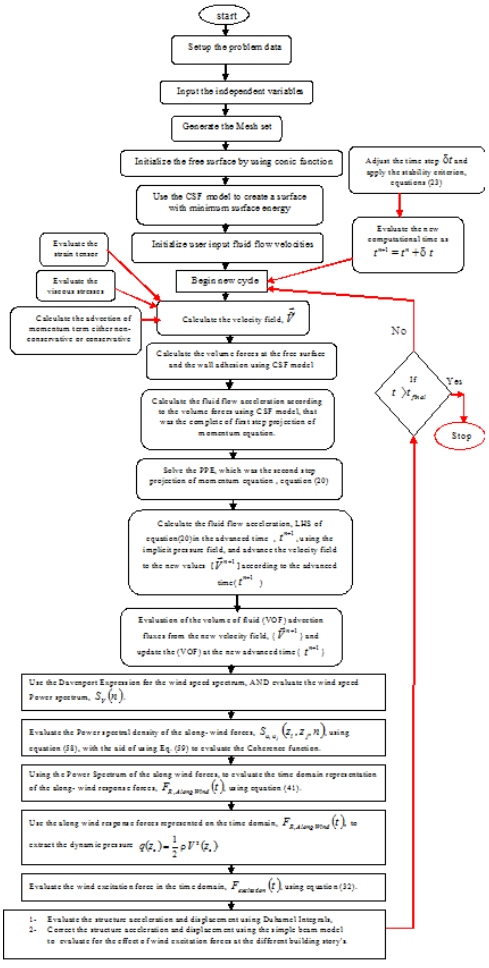

Figure 7. The Current Numerical Work Flow Chart

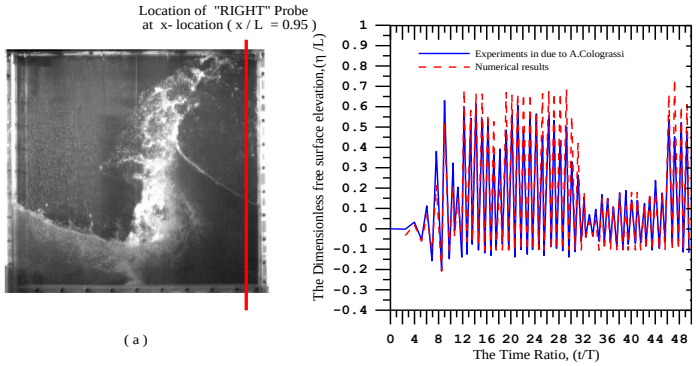

Figure 8. Time history of the dimensionless free surface elevation;
(a) The snapshot of the free surface, [38]. (the Red Line)points to the location of wave surface Probe (RIGHT)
(b) the comparison of the time history of the dimensionless Free Surface Elevation.

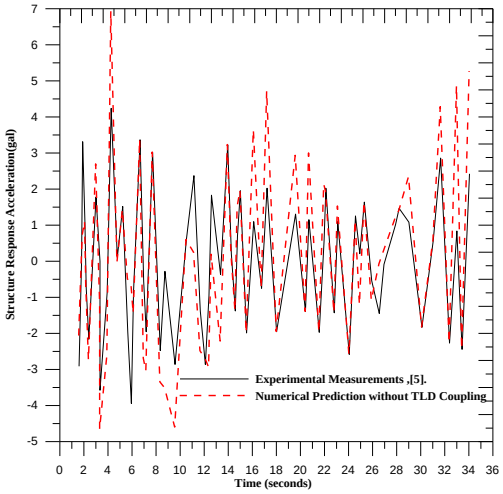

Figure 9. Time History of Building Response Acceleration.

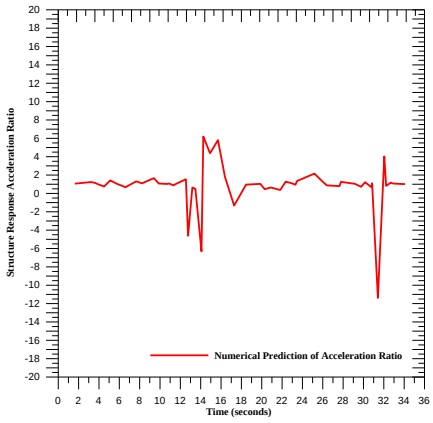

Figure 10. The Time History of Numerical Prediction of Acceleration Ratio

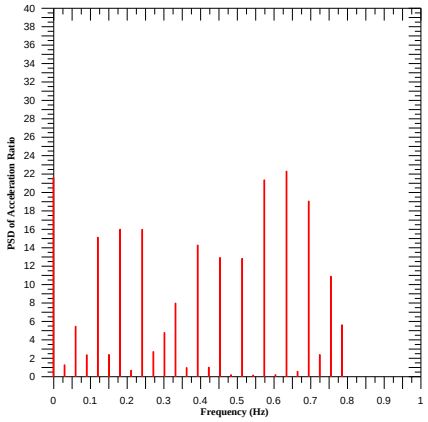

Figure 11. The Numerical Prediction of PSD of the Structure Acceleration Ratio.

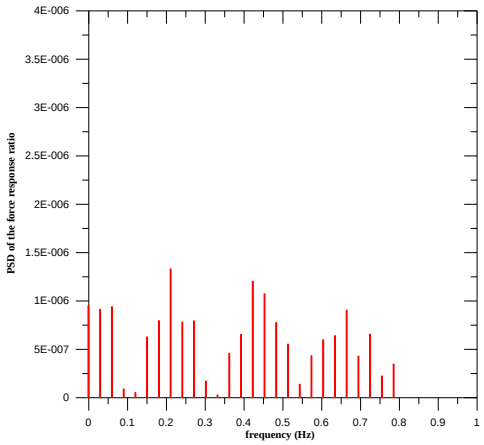

Figure 12. The Numerical Prediction of PSD of the Force response ratio of TMD having a mass equals to that of group of (10) TLD's.

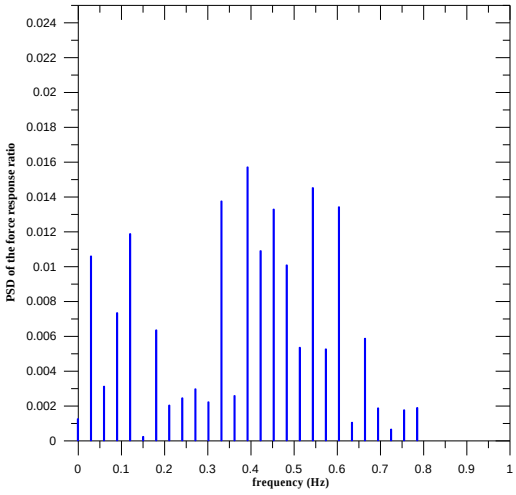

Figure 13. The Numerical Prediction of PSD of the Force response ratio of group of (10) TLD's.